MEASUREMENT OF VIBRATION PATTERNS USING
ELECTRO-OPTIC HOLOGRAPHY

Ryszard J. Pryputniewicz
Center for Holographic Studies and Laser Technology
Department of Mechanical Engineering
Worcester Polytechnic Institute
Worcester, MA 01609

Karl A. Stetson
Fiber Optics and Quantum Electronics
United Technologies Research Center
East Hartford, CT 06108

ABSTRACT

This paper describes the use of an Electro-Optic Holography system for measuring vibration patterns on diffusely reflecting objects. The system provides a high-quality display of J_o fringes for identifying modal frequencies and setting vibration levels after which image brightness data can be transferred to a host computer. A bias vibration is introduced into the illumination beam to shift the J_o fringes so that fringe shift algorithms can be used to determine vibration amplitude. Using this approach, high spatial density displacement fields for vibrating objects were obtained directly form the time-average interferograms recorded by the Electro-Optic Holography system. These results show good correlation with the reconstructions from the holograms and with the vibration characteristics predicted by the Finite Element Methods.

1. INTRODUCTION

In many design problems, it is inadequate merely to specify that load bearing components withstand only applied static loads. Rather, the designer must be concerned with cyclic displacements and stresses that will be introduced by periodic and/or random time varying loads acting on the component. There are many discrete frequencies at which the components will undergo large amplitude vibrations when acted upon by sustained time varying loads. These are the so called resonant, natural, or free vibration frequencies of the component. There is a distinct characteristic mode shape associated with each resonant frequency of the component as it vibrates. Most vibrations in machines and structures are undesirable because of the increased stresses and energy losses which accompany them. They should be eliminated, therefore, or reduced as much as possible by appropriate design. The analysis of vibrations has become increasingly important in recent years owing to the current trend toward higher-speed machines and lighter structures. Knowledge of the vibration characteristics of the components is essential for safe design of systems where the resonance of the component due to oscillating loads is possible. This knowledge can be obtained by conducting vibration analyses and by measuring vibration parameters of the components.

Today, the vibration analyses are to a great extent satisfied by application of the finite element methods (FEM)[1]. In these applications, the FEM are used to solve problems for which exact solutions do not exist, or are very difficult to obtain. Also, the FEM provide the only means to analyze complex three-dimensional structures, for which the response to the applied loads cannot be predicted by any other computational method. However, results obtained by the FEM depend on boundary conditions, rely greatly on the accurate knowledge

of material properties, depend on accurate representation of the structure's geometry, and are sensitive to the shape and the size of elements employed in modeling of the structure. All the information necessary to run the finite element models has been obtained, directly or indirectly, from experimental studies.

Currently, there are a number of experimental methods used to study vibrating structures. These methods are primarily based on the use of strain gauges and accelerometers and, in general, are invasive because they may affect the structure's response to the load. In 1965, however, the method of hologram interferometry was invented[2] and provided means for noninvasive measurement of vibrational characteristics of objects. Although this method provided means by which holograms of vibrating objects could readily be recorded, quantitative interpretation of interference fringes has traditionally been tedious and prone to considerable inaccuracy. This has led to the use of heterodyne and phase step methods to read out the interferometric fringes produced during reconstruction of holograms of vibrating objects. Although these methods[3-7] allowed high accuracy, 1/1000 and 1/100 of one fringe, respectively, in measurements of local phase differences, they still required physical recording of a permanent hologram in some type of photosensitive medium. These methods, therefore, do not qualify for fully automated vibration analysis. Recently, an automated method for processing of vibration fringes has been developed[8]. In this method, measurements of irradiances produced by mutual interference of the object and a reference fields are made electronically by a detector array. Processing of this interferometric information and display of the computational results are carried out concomitantly with measurements of irradiation. Because this method does not depend on recording of holograms in conventional media, but rather relies on electronic acquisition, processing, and display of optical interference information, it is called Electro-Optic Holography (EOH). In the following sections, application of EOH to fully automated, quantitative interpretation of holograms of vibrating objects is described. This description is based on the time-average method of recording of holograms.

2. ELECTRONIC RECORDING OF TIME-AVERAGE HOLOGRAMS

The image of a sinusoidally vibrating object can be described by the irradiance distribution, $I(x, y)$, at the detector array of a CCD camera in the EOH setup, such as[9]

$$I(x, y) = I_O(x, y) + I_R(x, y) + 2A_O(x, y)A_R(x, y)\cos[\Delta\phi(x, y)]M[\Omega(x, y)]. \qquad (1)$$

In Eq. 1, x and y identify coordinates of the detectors in the array, I_O and I_R denote irradiances of the object and reference fields, whose amplitudes are A_O and A_R, respectively, $\Delta\phi$ is the random phase difference between the two fields, M is a characteristic fringe function[10] that modulates the interference of the two fields due to the object's motion, and Ω is the fringe locus-function, constant values of which define fringe loci on the object's surface. The fringe-locus function is defined in terms of the interferometric fringe order n as

$$\Omega(x, y) = 2\pi n(x, y). \qquad (2)$$

Since I is measured at known coordinates x and y, Eq. 1 contains four unknowns, that is, irradiances (which are squares of the amplitudes) of the two fields, the phase difference between these fields, and the fringe-locus function. The goal is to determine Ω because it relates directly to displacements and deformations of the object[11].

In EOH, the random phase, $\Delta\phi$, is eliminated by recording sequentially four TV frames with an introduction of a 90° phase shift between each frame. This process can be represented by four simultaneous equations

$$I_1 = I_O + I_R + 2A_O A_R \cos(\Delta\phi)M(\Omega), \qquad (3)$$

$$I_2 = I_o + I_R + 2A_o A_R \sin(\Delta\phi)M(\Omega), \tag{4}$$

$$I_3 = I_o + I_R - 2A_o A_R \cos(\Delta\phi)M(\Omega), \tag{5}$$

$$I_4 = I_o + I_R - 2A_o A_R \sin(\Delta\phi)M(\Omega), \tag{6}$$

where the arguments (x, y) were omitted for simplification; it should be noted that a system of equations similar to Eqs 3 to 6 could be obtained using any value of the phase step, however, use of the 90° phase step results in the simplest computations.

Subtracting Eqs 3 and 5 and Eqs 4 and 6 gives the following two equations:

$$(I_1 - I_3) = 4A_o A_R \cos(\Delta\phi)M(\Omega), \tag{7}$$

$$(I_2 - I_4) = 4A_o A_R \sin(\Delta\phi)M(\Omega). \tag{8}$$

The EOH system is capable of operating in either a viewing mode, used for visual examination of the interference patterns, or a data mode, used for quantitative analysis of vibrating objects. The viewing mode produces an 8-bit image, while the data mode produces a 16-bit image. These images are produced by lookup tables resident in the EOH system. If the viewing mode is selected, the resident lookup table for the viewing mode is loaded into the operating system and, based on the input from Eqs 7 and 8, produces an image which can be expressed as

$$\sqrt{(I_1 - I_3)^2 + (I_2 - I_4)^2} = 4A_o A_R \mid M(\Omega)\mid. \tag{9}$$

This image is displayed live on a TV monitor and it can be stored in processor memory at any time. This storage can be of two types, as selected by menu options. If the image is to be recalled in the future for visual observation, then an 8-bit image is stored and occupies approximately one-quarter megabyte of memory - this is image storage. If the image is to be processed quantitatively, then the lookup table for the data mode is loaded into the operating system and, based on the input from Eqs 7 and 8, produces a data image which can be represented by

$$(I_1 - I_3)^2 + (I_2 - I_4)^2 = 16 I_o I_R M^2(\Omega). \tag{10}$$

This result is stored as the 16-bit data image and occupies one-half megabyte of memory - this is data storage. Either type of image may then be downloaded to the host computer's memory.

Equations 9 and 10 indicate that the viewing and the data images are proportional to the characteristic function and to the square of the characteristic function, respectively. The characteristic function is determined by the object's temporal motion[12], and for sinusoidal vibrations, assuming that the vibration period is much shorter then the TV framing time,

$$M[\Omega(x, y)] = J_o[\mid\Omega(x, y)\mid], \tag{11}$$

where J_o is the zero-order Bessel function of the first kind. Therefore, Eqs 9 and 10 become

$$\sqrt{(I_1 - I_3)^2 + (I_2 - I_4)^2} = 4A_o A_R \mid J_o(\mid\Omega\mid)\mid, \tag{12}$$

and

$$(I_1 - I_3)^2 + (I_2 - I_4)^2 = 16 I_o I_R J_o^2(\mid\Omega\mid), \tag{13}$$

respectively. Equation 12 results in a viewed image that is modulated by a system of fringes described by the zero-order Bessel function of the first kind, while Eq. 13 shows that the data image is modulated by the square of this function. Thus, centers of the dark fringes are located at those points on the object's surface where $J_o(|\Omega|)$ equals zero, as shown in Fig. 1. This figure indicates that the zero-order fringe is much brighter than the other J_o fringes. Since the zero-order fringes represent the stationary points on the vibrating object they allow easy identification of nodes. The brightness of other fringes decreases with increasing fringe order and can be directly related to the mode shapes. It should be noted that higher order zeros are nearly equally spaced giving the J_o function an almost periodic nature that is utilized in quantitative interpretation of images recorded by the EOH system as discussed in Section 3.
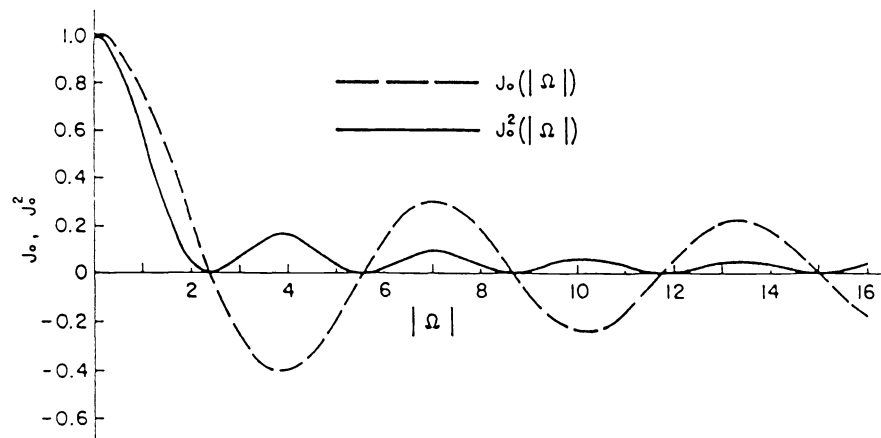

Fig. 1. The zero order Bessel function of the first kind and its square, defining location of centers of dark fringes seen during reconstruction of time-average holograms of vibrating objects.

In the EOH system, the data provided by the CCD camera are processed to produce results shown by Eq. 9 for every pixel in the image frame at the rate of 30 frames per second. Each frame contains 512x480 8-bit numbers corresponding to the irradiances shown by Eqs 3 to 6 so that each image consists of 245,760 points. For visual examination of the vibration modes, time-average hologram images corresponding to Eq. 9 are displayed on the TV monitor. These images are generated concomitantly by the pipeline processor of the EOH system. To produce data suitable for quantitative analysis of time-average holograms, 16-bit images represented by Eq. 10 are stored. These data are stored in two 8-bit bytes per pixel and produce a frozen image which can be displayed on the TV monitor one byte at a time, that is, either as a high-byte image or a low-byte image.

3. QUANTITATIVE INTERPRETATION OF
ELECTRONICALLY RECORDED TIME-AVERAGE HOLOGRAMS

3.1. Determination of the fringe-locus function

To interpret electronically recorded time-average holograms quantitatively, the argument of the J_o^2 function, appearing in Eq. 13, must be determined. One method to determine this argument, suitable for the time-average images recorded by EOH, was developed by Stetson and Brohinsky[8]. This method uses the fact that it is possible to shift J_o fringes in a manner similar to that in which phase modulation shifts cosinusoidal fringes

in conventional double-exposure hologram interferometry. In time-average holography, this is done by modulating the phase of either the object or the reference beams sinusoidally at the same frequency and phase as the object vibration. Such a process can be represented mathematically by addition of a phasor bias, B, to the argument of the Bessel function, resulting in the characteristic function

$$M[\Omega(x,y), B] = J_o[|\Omega(x,y) - B|].$$ (14)

For purposes of analysis, the object must be made to vibrate in only one vibration mode at a time so that the motions of its various parts are either in or out of phase with one another. If the phase of the sinusoidal beam modulation is adjusted to coincide with that of the object vibration, the phasor bias becomes a simple additive term within the argument of the Bessel function, that is,

$$M[\Omega(x,y), B] = J_o[|\Omega(x,y) - B|].$$ (15)

Therefore, Eq. 13 becomes

$$[I_1(x,y) - I_3(x,y)]^2 + [I_2(x,y) - I_4(x,y)]^2 = 16 I_0(x,y) I_R(x,y) J_o^2[|\Omega(x,y) - B|].$$ (16)

For comparison, the general equation representing the irradiance, I_h, of an image reconstructed from a time-average hologram is

$$I_h(x,y) = I_a(x,y) + I_m(x,y) J_o^2[|\Omega(x,y) - B|],$$ (17)

where I_a represents local average background irradiance from scattered light and I_m is the local maximum irradiance. Therefore, Eq. 16 is the special case of Eq. 17 with

$$I_h(x,y) = [I_1(x,y) - I_3(x,y)]^2 + [I_2(x,y) - I_4(x,y)]^2,$$ (18)

$$I_a(x,y) = 0,$$ (19)

and

$$I_m(x,y) = 16 I_0(x,y) I_R(x,y).$$ (20)

The output of the processor in the data mode, I_h, is stored in the host computer for different values of B, while I_a, I_m, and Ω constitute three unknowns, and the goal of the analysis is to determine Ω. Unfortunately, the Bessel function is not separable in terms of Ω and B, so a straightforward solution is not possible. However, the nearly periodic nature of the J_o function allows an approximate solution for the fringe-locus function[8]. This approximate solution recognizes that Eq. 17 is similar to the general equation for the irradiance distribution, I_h', for an image reconstructed from a conventional double-exposure hologram with cosinusoidal fringes, that is,

$$I_h'(x,y) = I_a(x,y) + I_m(x,y) \cos^2[\Omega'(x,y) - B],$$ (21)

where J_o^2 in Eq. 17 has been replaced by $\cos^2$ and Ω bas been replaced by Ω'.

Examination of Eq. 21 shows that it, just like Eq. 17, also has three unknowns: I_a, I_m, and Ω'. However, the $\cos^2[\Omega'(x,y) - B]$ term, appearing in Eq. 21, unlike the $J_o^2[|\Omega(x,y) - B|]$ term of Eq. 17, is separable in its component arguments. To facilitate solution of Eq. 21 for Ω, it is rewritten as

$$I_h'(x,y) = I_a'(x,y) + I_m'(x,y) \cos[2\Omega'(x,y) - 2B],$$ (22)

where

$$I'_a(x,y) = I_a(x,y) + \frac{I_m(x,y)}{2} \qquad (23)$$

and

$$I'_m(x,y) = \frac{I_m(x,y)}{2}. \qquad (24)$$

With three values of B, three simultaneous equations of the type of Eq. 22, can be solved uniquely for Ω'. The three simultaneous equations are

$$I'_{h_1}(x,y) = I'_a(x,y) + I'_m(x,y)\cos[2\Omega'(x,y)], \qquad (25)$$

$$I'_{h_2}(x,y) = I'_a(x,y) + I'_m(x,y)\cos[2\Omega'(x,y) - 2B], \qquad (26)$$

$$I'_{h_3}(x,y) = I'_a(x,y) + I'_m(x,y)\cos[2\Omega'(x,y) + 2B], \qquad (27)$$

corresponding to the zero-, positive-, and negative-shifts, respectively. Solution of Eqs 25 to 27 yields

$$\Omega'(x,y) = \frac{1}{2}\tan^{-1}\left\{ \left[\frac{1 - \cos(2B)}{\sin(2B)} \right] \frac{I'_{h_3}(x,y) - I'_{h_2}(x,y)}{2I'_{h_1}(x,y) - I'_{h_2}(x,y) - I'_{h_3}(x,y)} \right\}. \qquad (28)$$

If the three irradiance distributions $I_{h_1}(x,y)$, $I_{h_2}(x,y)$, and $I_{h_3}(x,y)$, corresponding to three time-average holograms, are substituted into Eq. 28 the result is $\Omega''(x,y)$. This value of Ω'' differs from the correct argument, Ω, of the J_o function, because of inequality between the J_o^2 and $\cos^2$ functions, and should be expressed as

$$\Omega''(x,y) = \Omega(x,y) + \epsilon(x,y), \qquad (29)$$

where ϵ is the error representing this difference.

Equation 28 yields values of Ω'' modulo 180°. By adding or subtracting 180°, depending on the sign of the numerator in Eq. 28, whenever the denominator is negative, Ω'' can be obtained modulo 360°. The image can be searched by the computer to locate discontinuities to define areas where the missing multiples of the 360° should be added to unwrap function Ω''. By further identifying pixels within the zero-order fringe, an overall level shift can be applied to make those pixels have values between ±180°.

Errors ϵ can be computed[8] for any value of Ω for specific values of B to create a lookup table, as discussed in Section 3.2. This lookup table is used to correct the values computed from Eq. 28 that have been unwrapped and level shifted. In this way, vibratory deformations can be obtained from time-average hologram reconstructions with little more mathematical computation than is required for static deformations. Once the correct values of Ω are determined, they can be used in any one of the equations for quantitative interpretation of time-average holograms[13].

3.2. Generation of a lookup table

The lookup table is computed from Eqs 17 and 28. First, three values of I_h are computed by using Eq. 17 for three values of B, for example, 0 and $\pm \pi / 3$, that is,

$$I_{h_1}(x,y) = I_a(x,y) + I_m(x,y) J_o^2[|\Omega(x,y)|], \tag{30}$$

$$I_{h_2}(x,y) = I_a(x,y) + I_m(x,y) J_o^2[|\Omega(x,y) - B|], \tag{31}$$

$$I_{h_3}(x,y) = I_a(x,y) + I_m(x,y) J_o^2[|\Omega(x,y) + B|]. \tag{32}$$

Substitution of these values into Eq. 28 yields

$$\Omega''(x,y) = \frac{1}{2}\tan^{-1}\left\{\left[\frac{1-\cos(2B)}{\sin(2B)}\right]\frac{J_o^2[|\Omega(x,y)+B|] - J_o^2[|\Omega(x,y)-B|]}{2J_o^2[|\Omega(x,y)|] - J_o^2[|\Omega(x,y)-B|] - J_o^2[|\Omega(x,y)+B|]}\right\}. \tag{33}$$

To construct a lookup table corresponding to a specific value of B, Eq. 33 is used to compute Ω'' for a desired range of values of Ω. Tabulating Ω versus Ω'' produces the lookup table for the given value of the bias vibration. If the magnitude of phase modulation of the bias vibration changes, new lookup table must be constructed.

4. EOH SYSTEM AND PROCEDURE

4.1. General description of the system

The EOH system used in this study is shown in Fig. 2. In this system, the laser output is divided into two beams by means of a continuously variable beamsplitter. One of these beams is directed via a piezoelectrically driven mirror and is shaped by the spatial filter beam expander assembly to illuminate the object uniformly; this mirror can be driven at the same frequencies as the object excitation to provide bias vibration. The other beam, also spatially filtered and expanded, is directed toward the reference input of the speckle interferometer by another piezoelectrically driven mirror which introduces 90° phase steps between consecutive frames. The speckle interferometer combines the object beam with the reference beam and directs them collinearly toward the detector array of the CCD camera. The camera detects the interference pattern and sends it to the pipeline processor. The sequential frames are processed as discussed in Section 2. All computations are done in a pipeline processor which operates under control of a host computer. The host computer also controls excitation of the object, coordinates it with the bias vibration imposed on the object beam, and keeps track of the 90° phase stepping between the frames.

By operating on each input image and its three predecessors, the pipeline processor produces a hologram, and this hologram is viewed concomitantly on the TV monitor. Such holograms are produced for the zero, as well as positive and negative bias vibrations, for each resonance frequency of the object; a procedure for setting up the bias vibration is discussed in Section 4.2. The resulting three electronic holograms are then processed by the host computer to determine spatial distribution of the displacement vectors which are viewed directly on the computer monitor.
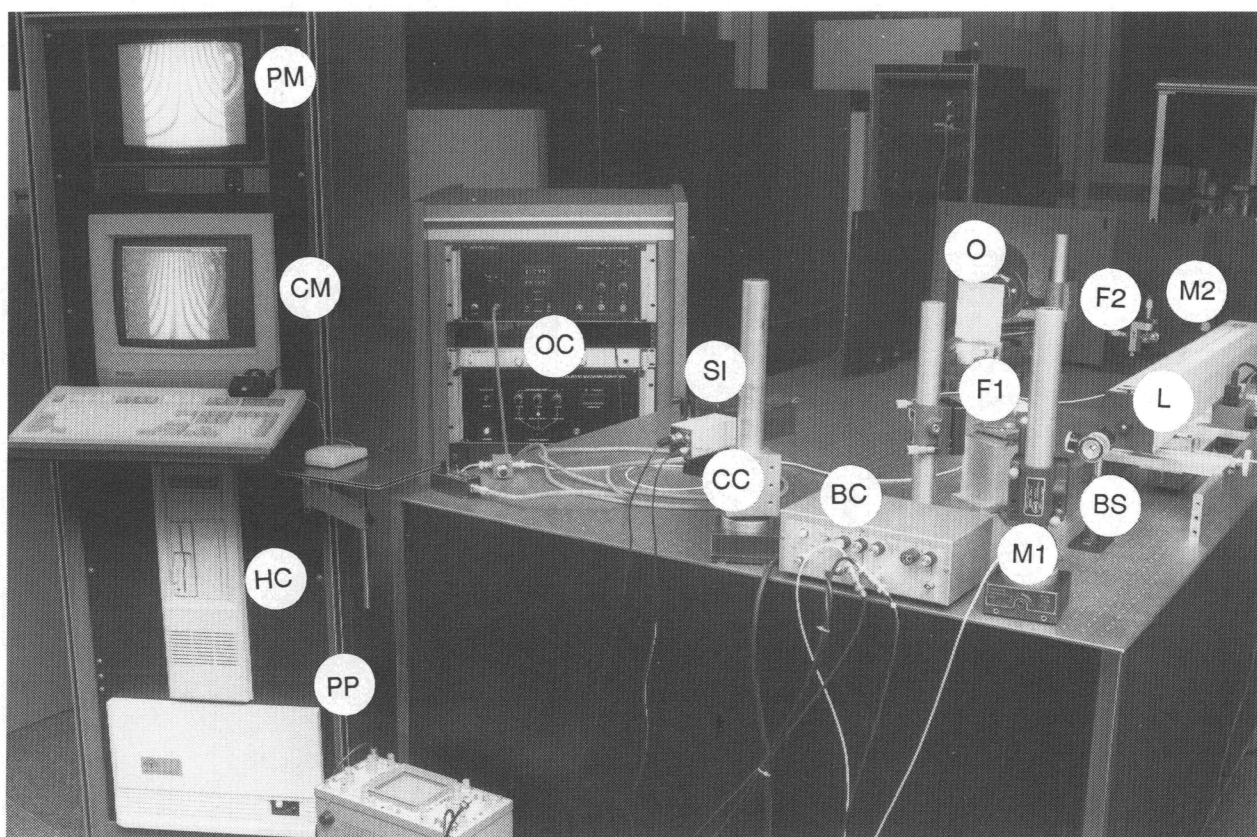
Fig. 2. The Electro-Optic Holography system: L is laser, BS is beamsplitter, M1 is piezoelectrically driven object beam mirror producing bias modulation, M2 is piezoelectrically driven reference beam mirror introducing 90° phase steps between consecutive frames, F1 and F2 are spatial filter beam expander assemblies, BC is bias modulation controller, O is object, OC is object vibration controller, SI is speckle interferometer, CC is CCD camera, PP is pipeline processor, HC is host computer, CM is computer monitor, and PM is processor monitor.

All results presented in this paper were obtained by studying vibrations of an aluminum cantilever plate which was rigidly fixed along its bottom edge. The plate was 115 mm wide, 135 mm high, and 2.3 mm thick. Representative results obtained using the EOH system are discussed in Section 5.

4.2. Setting the bias vibration

In order to interpret electronically recorded time-average holograms quantitatively, both the magnitude and the phase of the bias vibration must be known. One method to set the bias vibration is as follows.

Adjust object excitation so that several J_o fringes are seen across the object and the zero-order fringe is well identified. Then, increase magnitude of the bias vibration until the zero-order fringe is lost. Following this, adjust phase of the bias vibration until the zero-order fringe is regained and its width is maximum. At this point, phase of the bias modulation equals the phase of the vibrating object.

Next, turn off object excitation and reduce magnitude of the bias vibration to zero - do not, however, change the bias phase! Then, slowly increase magnitude of the bias vibration until the entire object goes black, that is, when the first null of J_o occurs. At this point, the value of B is 2.4048. Record the voltage output of the bias

modulation controller for this condition and reset it by a scaling factor. The scaling factor is the desired magnitude of the bias vibration (for example, $\pi/3$) divided by 2.4048, the argument for the first zero of the J_o. The phase of this bias vibration should be recorded; it corresponds to the positive-shift modulation. This completes calibration of the magnitude and the phase of the bias vibration and the sequence of the three holograms can be recorded. Before this is done, the bias excitation should be turned off, the object excitation should be turned on, and the excitation magnitude should be adjusted to the desired level.
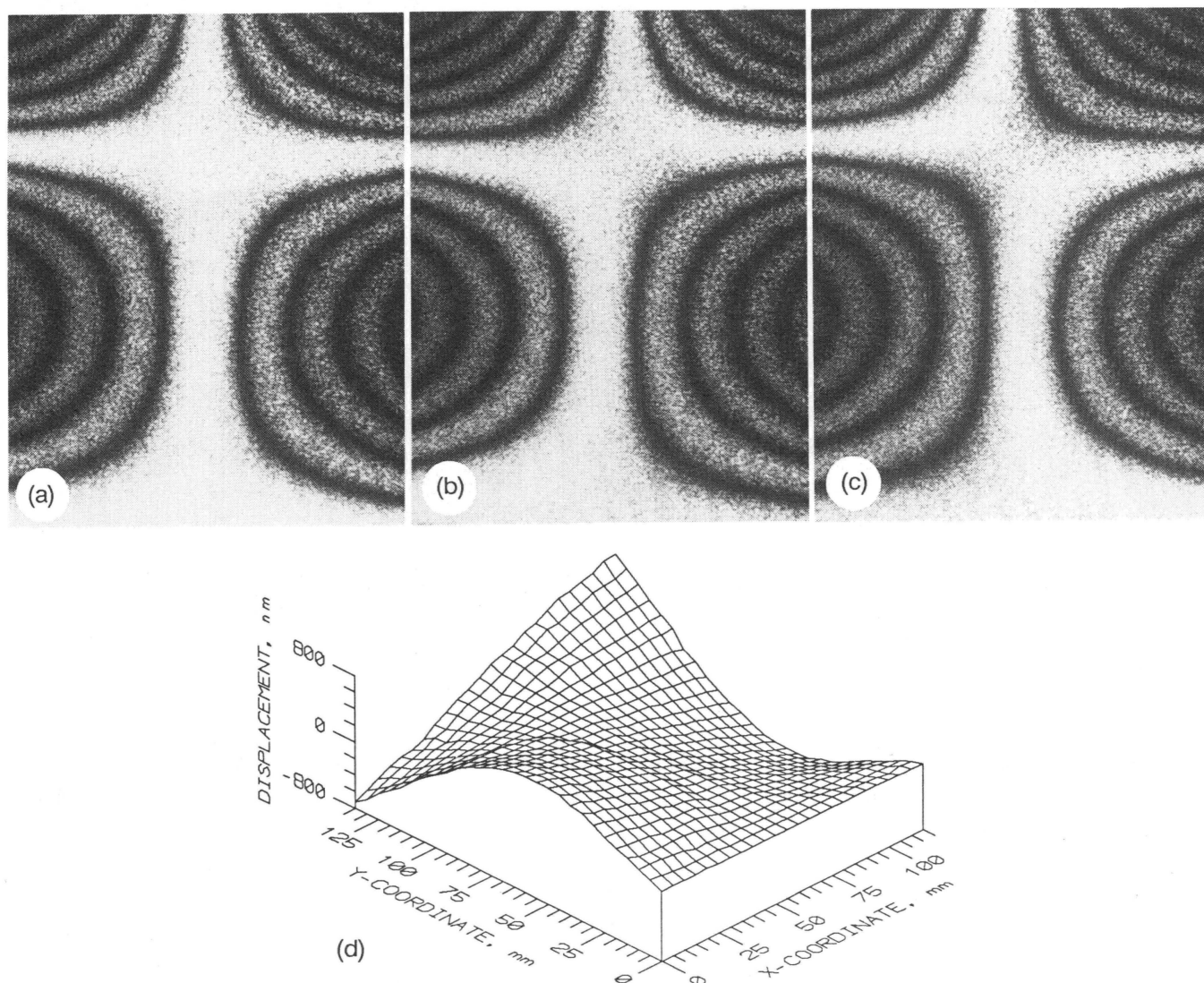

Fig. 3. Cantilever plate vibrating at 966 Hz: (a) image of the plate and the fringe pattern produced by the EOH system during the time-average recording of the plate vibrating at its resonance without bias modulation of the object beam, (b) same plate and vibration as in (a) but with a bias modulation added to the object beam at the object's vibration frequency, (c) same plate and vibration as in (a) but with a bias modulation added to the object beam at 180° with respect to (b), (d) wire frame representation of displacements computed from the images shown in (a) to (c).

When the desired object excitation is achieved, the first time-average hologram is recorded without the bias excitation; this is the zero-bias modulation. Then, the second hologram is recorded after switching on the bias excitation with the magnitude and phase as set above; this is the positive-shift bias modulation. Finally, the

phase of the bias excitation is shifted 180° with respect to that used during recording of the second hologram, the bias magnitude is kept the same, and the third hologram is recorded; this is the negative-shift bias modulation. Irradiances of the three time-average holograms recorded in this way are represented by Eqs 30 to 32, respectively. Note that the bias vibration should be recalibrated at each vibration frequency of the object.

5. RESULTS AND DISCUSSION

Typical results obtained using the EOH system are shown in Figs 3 to 5. All interferograms shown in these figures were produced electronically, as discussed in Section 4, and were photographed directly from the displays on the TV monitor. All wire frame displacement plots were based on irradiances measured from the sets of three holograms corresponding to the zero, the positive, and the negative bias modulations added to the object beam at the object's vibration frequency.
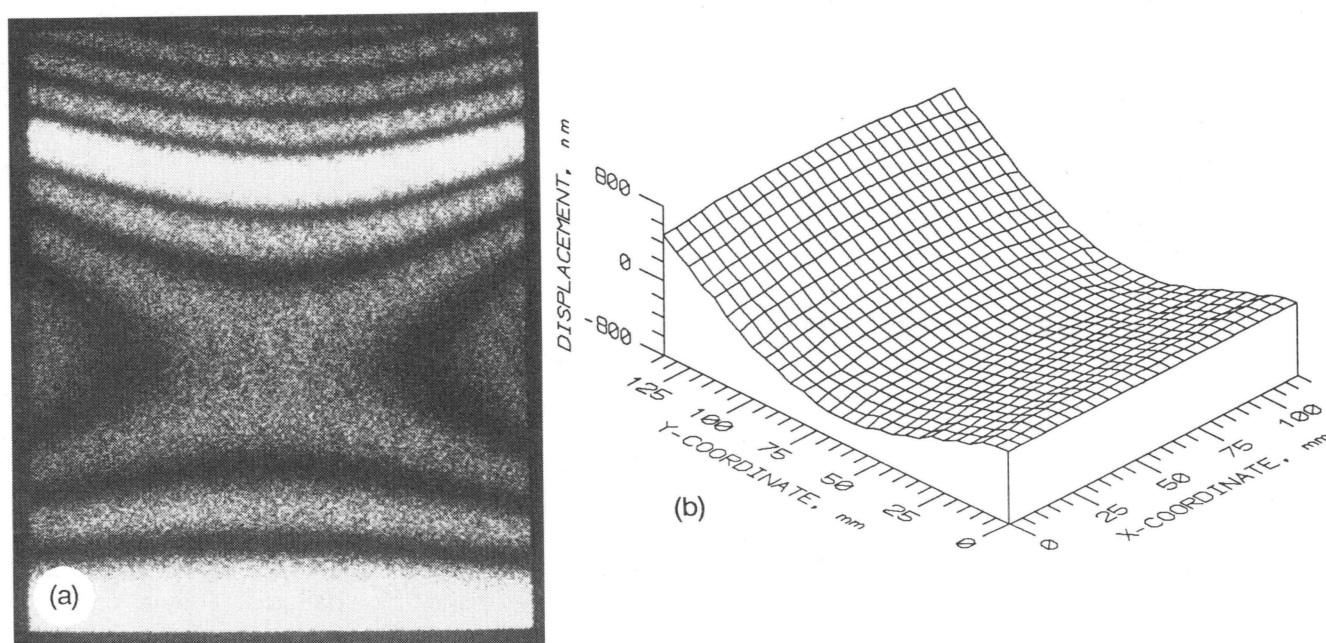

Fig. 4. Cantilever plate vibrating at 601 Hz: (a) image of the plate and the fringe pattern produced by the EOH system during the time-average recording of the plate vibrating at its resonance without bias modulation of the object beam, (b) wire frame representation of displacements computed from the images recorded by the EOH system.

It should be noted that because of the plate's aspect ratio only (250x400=) 100,000 pixels out of the total available of (512x480=) 245,760 pixels were used in the interpretation of the images produced by EOH. Furthermore, to produce visually acceptable plots, wire frame grid of 5x5 mm for representation of displacements was selected. In this way, displacements at only a very small number of points (24x28 = 672), out of the total of 100,000 points considered on the object, were displayed.

Figure 3 shows the cantilever plate vibrating in its second torsional mode at 966 Hz. More specifically, Fig. 3a shows the time-average hologram produced by the EOH system without bias modulation of the object beam, whereas Figs 3b and 3c show the holograms with equal positive and negative bias modulations added to the object beam at the object's vibration frequency, respectively. Note the symmetric location of the zero-order fringe in Fig. 3a and the offset in the symmetry, due to the bias modulation, in Figs 3b and 3c.

Based on the irradiance values from the corresponding points in Figs 3a to 3c, displacements were computed as a function of x and y coordinates on the vibrating plate. These displacements are shown in Fig. 3d and correlate well with the image displayed in Fig. 3a. The results obtained using the EOH agree well with the results produced by the FEM which indicate resonance frequency of 982 Hz for the second torsional mode.
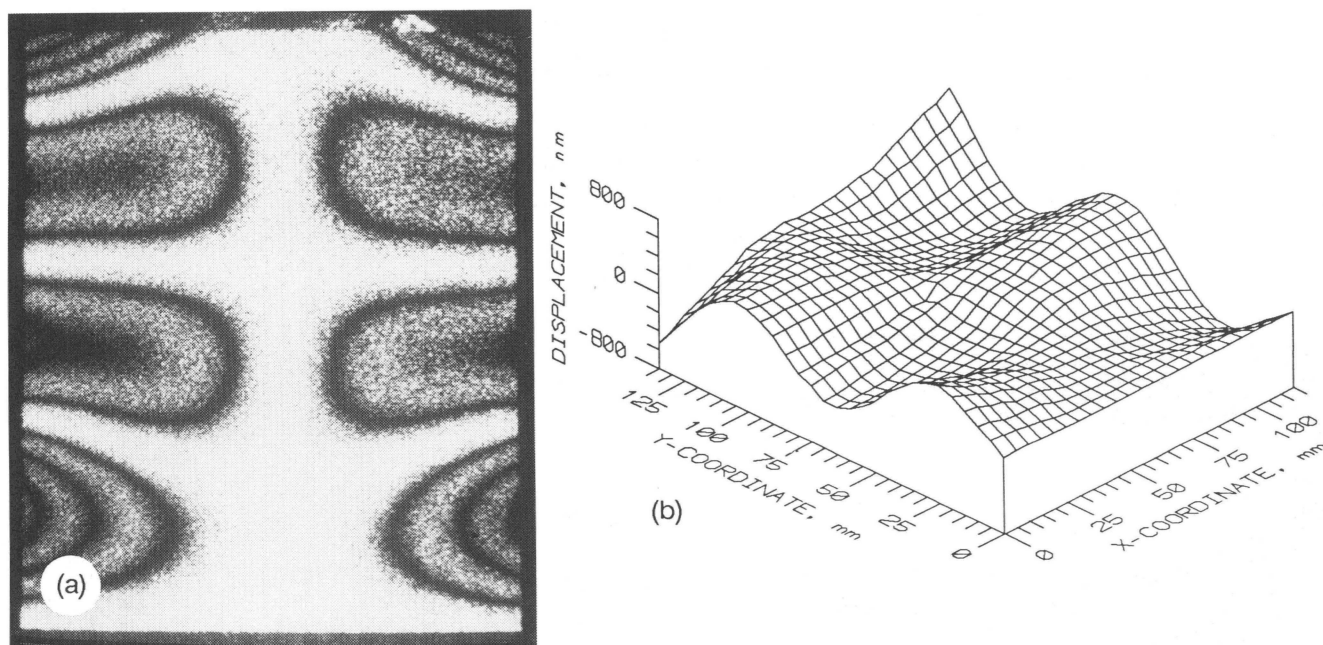

Fig. 5. Cantilever plate vibrating at 3787 Hz: (a) image of the plate and the fringe pattern produced by the EOH system during the time-average recording of the plate vibrating at its resonance without bias modulation of the object beam, (b) wire frame representation of displacements computed from the images recorded by the EOH system.

Results for the second flexural mode, recorded at 601 Hz, are shown in Fig. 4, while Fig. 5 shows the same plate vibrating at 3787 Hz. In both cases, the wire frame displays of the displacements computed from holograms recorded by the EOH system correspond well with the images of the fringe patterns. They also show acceptable correlation with the FEM computed frequencies of 623 Hz and 3830 Hz, respectively.

6. CONCLUSIONS

The results presented in this paper show that the EOH system effectively records high-quality concomitant time-average holograms of vibrating objects. These results also show that displacements can be extracted from such electronically recorded holograms by a method analogous to optical fringe shifting. The equivalents to optical phase shifts are generated by applying a vibratory phase modulation to the beam object beam at the object's vibration frequency. The amplitude of the modulation must be known, and the phase must match that of the object whose vibrations are to be measured. The resulting J_o fringes, with varying levels of bias vibration, are analyzed as though they were cosine fringes, and the results are corrected to compensate for the differences between the J_o^2 and the $\cos^2$ functions.

Using the EOH, results are obtained in a truly totally automated manner. The interferometric information is recorded electronically at the rate of 30 frames per second, it is processed in a pipeline fashion, and produces

results which have very high spatial density - currently at up to 512x480 points per frame. These results correlate well with the fringe patterns observable during reconstructions of time-average holograms and they also correlate well with the FEM predictions of object's vibration characteristics.

It should be noted that the EOH is not only capable of operating on vibration interference patterns, but it is also capable to operate on static interference patterns.

Currently, work is underway to merge, within the host computer, the vibrational displacements determined by the EOH system with the computational procedures of the FEM. This feat will result in a hybrid system which will allow totally automated, quantitative analysis of structural deformations.

7. REFERENCES

1. R. J. Pryputniewicz, "Holographic and finite element studies of vibrating beams," *Optics in Engineering Measurement*, SPIE-599:54-62 (1985).

2. R. L. Powell and K. A. Stetson, "Interferometric vibration analysis by wavefront reconstruction," *J. Opt. Soc. Am.*, 55:1593 (1965).

3. B. Ineichen and J. Mastner, "Vibration analysis by stroboscopic two-reference-beam heterodyne holographic interferometry," *Optics Applied to Metrology*, SPIE-210:207-212 (1980).

4. K. A. Stetson, "Method of vibration measurements in heterodyne interferometry," *Opt. Lett.*, 7:233-234 (1982).

5. P. Hariharan and B. F. Oreb, "Stroboscopic holographic interferometry: application of digital techniques," *Opt. Commun.*, 59:83 (1986).

6. S. Nakadate, "Vibration measurement using phase-shifting time-average holographic interferometry," *Appl. Opt.*, 25:4162-4167 (1986).

7. R. J. Pryputniewicz, "Vibration studies using heterodyne hologram interferometry," *Industrial Laser Interferometry II*, SPIE-955:154-161 (1988).

8. K. A. Stetson and W. E. Brohinsky, "Fringe-shifting technique for numerical analysis of time-average holograms of vibrating objects," *J. Opt. Soc. Am. - A*, 5:1472-1476 (1988).

9. R. J. Pryputniewicz, "Quantitative interpretation of time-average holograms in vibration analysis," *Optical metrology*, NATO ASI Series E: Applied Sciences - No. 131, Martinus Nijhoff Publishers, Dordrecht, The Netherlands, pp. 296-316 (1987).

10. K. A. Stetson, "Effects of beam modulation on fringe loci and localization in time-average hologram interferometry," *J. Opt. Soc. Am.*, 60:1378 (1970).

11. R. J. Pryputniewicz, "Review of methods for automatic analysis of fringes in hologram interferometry," *Interferometric Metrology*, SPIE-816:140-148 (1987).

12. K. A. Stetson, "Holographic vibration analysis," in *Holographic Nondestructive Testing*, R. K. Erf, ed., Academic Press, New York, pp. 181-220 (1974).

13. R. J. Pryputniewicz, "Time-average holography in vibration analysis," *Opt. Engrg.*, 24:843 (1985).